Journal of Cancer Research and Clinical Oncology (2019) 145:1191–1200
https://doi.org/10.1007/s00432-019-02866-7

ORIGINAL ARTICLE – CANCER RESEARCH

Ultrasound-targeted microbubble destruction improved the antiangiogenic effect of Endostar in triple-negative breast carcinoma xenografts

Yang Jing[1] · Zhang Xiu-Juan[2] · Cai Hong-Jiao[3] · Chen Zhi-Kui[2] · Qian Qing-Fu[2] · Xue En-Sheng[2] · Lin Li-Wu[2]

Received: 10 September 2018 / Accepted: 16 February 2019 / Published online: 25 February 2019

Abstract

Purpose Ultrasound-targeted microbubble destruction (UTMD) has been reported to be a meritorious technique for drug targeting delivery. In this study, we aimed to evaluate the synergistic antiangiogenic effect of UTMD combined with Endostar on triple-negative breast carcinoma tumors.

Materials and methods The lipid-shelled microbubbles (MBs) conjugated with Endostar were constructed using a biotin–avidin bridging chemistry method, and the morphological characteristics and drug-conjugating content were determined. MBs were administered intravenously to nude mice bearing MDA-MB-231 breast carcinoma xenografts and ultrasound exposure followed. The tumor microcirculation was observed by contrast-enhanced ultrasonography (CEUS) and the Endostar biodistribution was detected by enzyme-linked immunosorbent assay. Twenty-four breast carcinoma-bearing nude mice were divided into four groups. After treatment, every 3 days for 15 days the in vivo antitumor effects were assessed by calculating the tumor growth inhibition rate (TGIR). The tumor microcirculation was observed by CEUS, the tumor microvessel density (MVD) was calculated by immunohistochemistry under a microscope, and the vascular endothelial growth factor (VEGF) gene expression was detected by real-time quantitative polymerase chain reaction.

Results The prepared Endostar-conjugated MBs were round and well-dispersed with a mean size of 2.8 ± 0.7 μm and a drug conjugating content of 800.72 ± 70.53 μg/10^8 MBs. UTMD blocked the tumor microcirculation, and improved Endostar release in the targeted tumor tissue with a drug content of 1.12 ± 0.43 μg/gram protein, which was about three times higher than that in Endostar group or Endostar conjugated MBs group. Endostar-conjugated MBs combined with UTMD treatment achieved the optimal antitumor effects in vivo with a TGIR of 46.29%, and apparent antiangiogenic effects with minimal tumor blood perfusion, MVD and VEGF gene expression level.

Conclusion UTMD can improve Endostar delivery in the targeting tumor tissue and mediate synergistic antiangiogenetic and antitumor effects, which may be a potential therapeutic strategy for refractory breast cancer.

Keywords Ultrasound-targeted microbubble destruction · Endostar · Antiangiogenesis · Triple-negative breast carcinoma · Vascular endothelial growth factor

Introduction

Triple negative breast cancer (TNBC), one of the refractory breast cancers, occurs in approximately 15%–18% of breast cancer patients. Due to the absence of estrogen receptors, progesterone receptors, and human epidermal growth factor receptor 2 (HER2) expression, it is insensitive to endocrine as well as HER2-targeted therapy (Keam et al. 2011; Bauer et al. 2007; Dent et al. 2007; De Temmerman et al. 2011). In addition, owing to its inherent instability, TNBC has a propensity for rapidly developing multiple drug resistance,

The authors Yang Jing, Zhang Xiu-Juan and Cai Hong-Jiao have contributed equally to this article.

✉ Chen Zhi-Kui
jimchen2003@163.com

[1] Department of Pharmacy, Affiliated Union Hospital of Fujian Medical University, Fuzhou, China

[2] Department of Ultrasound, Affiliated Union Hospital of Fujian Medical University, Fuzhou, China

[3] Fisheries College of Jimei University, Xiamen, China

including natural and acquired forms, leading to a poor prognosis.

The genesis, growth, and transference of tumors requires an efficient blood supply (Sharma et al 2011). Antiangiogenic agents can increase the tumor sensitivity to chemotherapeutics, reduce the tumor vessel density and result in tumor shrinkage (Fukumura et al. 2007; Carmeliet et al. 2011). Accordingly, the molecular targeting therapy for angiogenesis may be a promising strategy for TNBC therapy.

Endostatin is a 20 kDa C-terminal fragment of collagen XVIII that can inhibit proliferation and migration of vascular endothelial cells, induce cell apoptosis (O'Reilly et al. 1997; Luo et al. 2015), and exhibit significant antiangiogenetic effects (Matsumoto etal. 2014; Karaca et al. 2012). By adding an additional nine-amino acids to the N-terminal of endostatin, the recombinant Endostar has improved stability and bioactivity and has been widely used in the clinic as a combined modality therapy for malignant tumors (Xu et al. 2013).

Yuan, et al. reported that intravenous injection of Endostar combined with chemotherapy can improve the survival rate of patients with liver metastases in advanced HER-2 negative breast cancer (Yuan et al. 2010). However, similar to most protein drugs, systemic administration of Endostar has certain limitations. Firstly, due to the short plasma half-life (10.7 h), the plasma drug concentration fluctuates constantly. Secondly, in one course of treatment, the patients need intravenous injection of Endostar daily for 14 days, and the treatment procedure may require 2–4 courses. This raises the medical fees and causes patient noncompliance. Thirdly, after intravenous injection, Endostar is distributed throughout the body and does not accumulate in the targeted tumor, leading to adverse reactions, especially in the cardiovascular system. Therefore, a modified administrative approach for Endostar would be of great significance.

In this study, lipid-shelled microbubbles (MBs) were conjugated with Endostar using biotin–avidin bridging chemistry. A human breast carcinoma MDA-MB-231-bearing nude mouse model was established and the biological effects of ultrasound-targeted microbubble destruction on tumor microcirculation and drug biodistribution were studied. Meanwhile, the antiangiogenic and antitumor effects of different treatments were investigated.

Materials and methods

Materials

Drugs and reagents

NHS-ester biotinylation, Avidin, 1,2 Distearoyl-sn-glycero-3-phosphatidylcholine (DSPC) (Sigma-Aldrich, USA), Distearoyl-sn-glycero-3-phosphoethanolamine-*N*- [Methoxy (Polyethyleneglycol)-2000](DSPE-PEG2000), 2-distearoyl-sn-glycero-3- phosphoethanolamine-N-[Biotinyl (Polyethylene Glycol) 2000] (DSPE-PEG2000-Biotin) (Avanti Polar Lipids Inc, USA), Endostar (Simcere Medgenn Company, China), Endostar ELISA Kit (Xitang Biotechnology Co., Ltd., Shanghai, China), acoustic contrast agent SonoVue (Bracco SpA, Milan, Italy), CD31 polyclonal antibodies (Maixin-Bio, Fuzhou, China). All other reagents were of analytical grade and were used as received.

Tumor cell line and animals

The human MDA-MB-231 breast cancer cell line was purchased from the Shanghai Institute of Cell Biology (Shanghai, China). Specific pathogen-free (SPF) BALB/c nu–nu female nude mice, 5-week-old and 16–18 g, were purchased from the SLAC Company (Shanghai, China). The mice were kept in a designated pathogen-free animal room and allowed to feed and drink freely. Handling of the animals was conducted strictly in accordance with the guidelines for animal experiments stipulated by Fujian Medical University, Fuzhou, Fujian, China.

Preparation of biotinylated Endostar

Biotin-*N*-hydroxy succinimide ester and Endostar were sufficiently mixed at a molar ratio of 15:1, and then incubated at 4 °C for 24 h before terminating with 10 mol/L glutamate. The reaction mixture was transferred into an ultrafiltration tube (filtration molecular weight 5 kDa), centrifuged at 10,000*g* at 4 °C for 20 min, and then washed three times with phosphate buffer saline (PBS) (Wu et al. 2010).

Preparation of MBs

DSPC, DSPE-PEG2000 and DSPE-PEG2000-Biotin (90:5:5, molar ratio) were added to 2 mL of PBS (0.01 mol/L, pH 7.2). The lipid suspension was maintained at 60 °C in a water bath, sonicated to clarity using a bath sonicator (KQ-300DE, Kunshan, China) at 40 kHz and 120 W three times for 3-min. A dispersed lipid suspension, 0.5 mL, was added to a 2 mL vial, and the air in the vial was replaced by perflutren gas. The sealed vial was fixed in a VialMix Mixer Shaker (Bristol Myers Squibb, USA) and mechanically agitated at a frequency of 4000 times per minute for 40 s to form the biotinylated MBs. The prepared MBs were diluted with 2.5 mL PBS, centrifuged at 300*g* for 3-min, and the floating MBs were collected. After three washes, the number of MBs formed was calculated using a microscope and a cell counting plate. Avidin was added at a concentration of 50 μg per 10^8 MBs and the mixture incubated for 15 min at room temperature with gentle

shaking. The avidin-bound biotinylated MBs were separated from free avidin by centrifugation and washed three times. The biotinylated Endostar was added to the avidin-bound biotinylated MBs suspension at an equal molar ratio to the DSPE-PEG2000-Biotin. The mixture was incubated for 30 min at room temperature with gentle shaking and washed three times to remove the free drug to obtain the Endostar-conjugated MBs. Fluorescein isothiocyanate (FITC)-labeled Endostar was used to prepare the fluorescent MBs. Unconjugated MBs that had no Endostar were also prepared as a control (Wen et al. 2014; Molinari et al. 2014; Delalande et al. 2013).

Characterization of MBs

The morphological characteristics of the prepared MBs were determined using fluorescence microscopy (Olympus, Tokyo, Japan). Briefly, 20 μL of a diluted MBs suspension was added to a cell counting plate to detect the MBs size, amount, and fluorescence at 400 × magnification.

Measurement of endostar content of MBs

The quantity of Endostar bound to the MBs was determined by ELISA. Briefly, after incubation with biotinylated Endostar for 30 min, the Endostar-conjugated MBs suspension was centrifuged at 160*g* for 5 min, and the lower solution was collected to detect the concentration of unconjugated Endostar. The Endostar-conjugating content was calculated using the following formula:

$$[\text{Conjugated Endostar content per } 10^8 \text{ MBs}] = ([\text{ total Endostar used}] - [\text{unconjugated Endostar}])/[\text{amount of } 10^8 \text{ MBs}].$$

Establishment of animal model

The human breast cancer MDA-MB-231 cell line was subcultured in L15 medium containing 10% fetal bovine serum at 37 °C while exposed to 5% CO_2 with a saturated humidity. After amplification, the cell suspension was prepared at a density of 5×10^7 cells/mL in a PBS and Matrigel mixture (1:1, volume ratio) in an ice bath. We injected 0.1 mL of the cell suspension into the right armpits of the nude mice to prepare the breast cancer xenograft and regularly monitored tumor growth.

Influence of ultrasound-targeted microbubble destruction on tumor microcirculation

Twelve breast cancer-bearing nude mice with a tumor diameter about 1.5 cm were randomly divided into two groups of six each to investigate the influence of UTMD on tumor microcirculation. After ether inhalation anesthesia, the mice were administered an intravenous injection of SonoVue at a dose of 5 mL/kg, and then exposed to ultrasound irradiation using an ultrasound treatment device (838A-H-O-S, Shengxiang Ultrasonic, Shenzhen, China). The acoustic beam produced by the ultrasound probe was cylindrical with a sectional area of 8.0 cm^2. A water balloon was placed on the surface of the probe, and the ultrasound coupling gel was applied to remove the gas between the probe and the tumor. The ultrasound exposure (frequency of 840 kHz) was performed with a power of 0.75 w/cm^2 for 2 min (an irradiation of 10 s and an interval of 10 s for six cycles). Thirty minutes later, contrast-enhanced ultrasonography (CEUS) was performed by intravenous bolus injection of 5 mL/kg of SonoVue and scanning by PLT-805AT probe (central frequency, 8.0 MHz) on a clinical diagnostic ultrasound system (Aplio 500, Toshiba). Three hours after UTMD, CEUS was repeated to evaluate the tumor blood reperfusion. The raw data were recorded and further analyzed using TCA and Modelisation software (Toshiba). After drawing a region of interest (ROI) of the tumor, the time intensity curve (TIC) was created, and the CEUS parameters including Peak Intensity (PI), Time to Peak (TP), Mean Transit Time (MTT), Area Under the Curve (AUC), Area Under the Curve-Wash In (AUC-WI) and Area Under the Curve-Wash Out (AUC-WO) were applied to evaluate the tumor microcirculation.

Effect of UTMD on drug biodistribution

Eighteen breast cancer-bearing nude mice with a tumor diameter about 1.5 cm were randomly divided into three groups of six each: Endostar, Endostar-conjugated MBs (EM), and Endostar-conjugated MBs combining with UTMD (EMUTMD) groups. The drugs were intravenously administered at an Endostar dosage of 10 mg/kg, while in the EMUTMD group, the mice received additional ultrasound exposure with the method mentioned above. Thirty minutes later, the mice were euthanized by exsanguination, followed by intravenous injection of 3 mL of saline to flush the circulatory system. The tumors were removed, homogenized with a tissue digesting solution, centrifuged at 10,000*g* for 30 min, and then the supernatant was sampled to detect the Endostar content by ELISA.

In vivo antitumor effects

Twenty-four mice with a tumor diameter of 1.0–1.2 cm were randomly divided into four groups of six mice: untreated (control), Endostar, EM, and EMUTMD groups. In three treatment groups, Endostar was intravenously injected at a

dose of 10 mg/kg, while in the EMUTMD group, the mice received additional ultrasound exposure with the method mentioned above. The treatments were repeated five times, every 3 days. On day 18, CEUS was performed to evaluate the microcirculation perfusion of the tumors. After that, the mice were euthanized, the tumors were excised, and the TGIR was calculated using the following formula:

$$\mathrm{TGIR}(\%) = (1 - \text{mean tumor mass of treatment group} / \text{mean tumor mass of control group}) \times 100\%$$

Tumor microvessel histopathological examination

Tumor tissue was fixed with 10% formaldehyde, conventionally dehydrated, embedded in paraffin, serially sectioned, and then probed using immunohistochemistry. The expression of CD31 by the tumor vascular endothelial cells was detected using the Streptavidin-Peroxidase (SP) method (Zhai et al. 2013). The microvessels in five microscopic fields were counted at 100 × magnification, and the mean value was calculated for MVD evaluation.

Determination of VEGF expression level

Total RNA was extracted from tumor tissues using a kit according to the manufacturer's instructions and subsequently reverse transcribed to cDNA. The gene expression of VEGF was determined using qPCR with an ABI 7300 PCR instrument. Each reaction was run in triplicate. The reaction mixture contained 2 µL and 1.6 µL of the template and primer, respectively, in a final reaction volume of 25 µL. The primer pair sequences for VEGF were 5′-GGC AGA ATC ATC ACG AAG TGG-3′ (sense) and 5′-GTG AGG TTT GAT CCG CAT AAT CT-3′ (antisense) while those for actin were 5′-ATT CCT ATG TGG GGG ACG A-3′ (sense) and 5′-GCT GGG GTG TTGA AGG TCT-3′ (antisense) with an expected product size of 236 and 241 bp, respectively. The PCR cycling parameters were 95 °C for 30 s, followed by 40 cycles of 95 °C for 5 s and 60 °C for 31 s. The data were obtained as average CT values normalized to the control expressed as ΔCT, and differences in expression changes in gene transcripts of the breast carcinoma control and treatment groups are shown as $2^{\Delta\Delta CT}$.

Statistical analysis

All data are presented as mean ± standard deviation and were analyzed using the statistical package for the social sciences (SPSS) version 19 statistical software. A single-factor analysis of variance (ANOVA) was performed to compare the Endostar distribution, tumor mass, CEUS parameters, MVD, VEGF gene expression level in different groups, and $P < 0.05$ was considered statistically significant and $P < 0.01$ very statistically significant. If ANOVA demonstrated a significant difference among the groups, post-hoc Tukey's test adjusting for multiple comparisons was performed to determine where the differences resided.

Results

Characteristics of MBs

The prepared unconjugated MBs were well-dispersed with a mean size of 2.9 ± 1.0 µm and a density of $(4.5 \pm 0.8) \times 10^8$ MBs/mL under microscopy (Fig. 1). The Endostar-conjugated MBs were also well-dispersed, with a concentrated size distribution of 2.8 ± 0.7 µm, and production of $(2.1 \pm 0.6) \times 10^8$ MBs/mL. The Endostar conjugated onto the shell of the MBs emitted brilliant green fluorescence (Fig. 2), and the drug-conjugating content was 800.72 ± 70.53 µg/10^8 MBs.

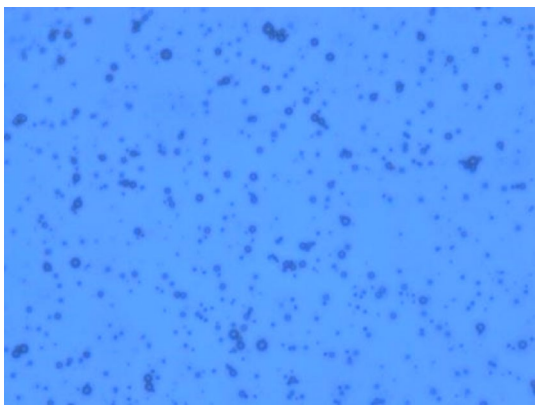

Fig. 1 The unconjugated MBs photo under microscopy (400×)

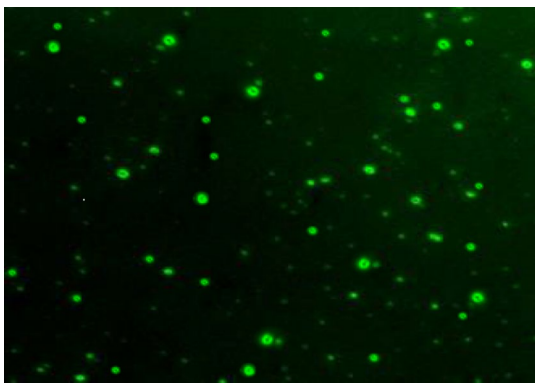

Fig. 2 The Endostar conjugated onto the shell of MBs emitted green fluorescence under fluorescence microscopy (400×)

Effect of UTMD on tumor microcirculation

Under CEUS, the tumors in the control group displayed intense and homogeneous enhancement. In the UTMD group, 30 min after UTMD, enhancement of the whole tumor throughout the CEUS procedure was not seen (Fig. 3). However, 3 h after UTMD, the tumor blood perfusion resumed, the TP, MTT, PI, AUC, AUC-WI, AUC-WO measured were similar to those of the control group (Table 1).

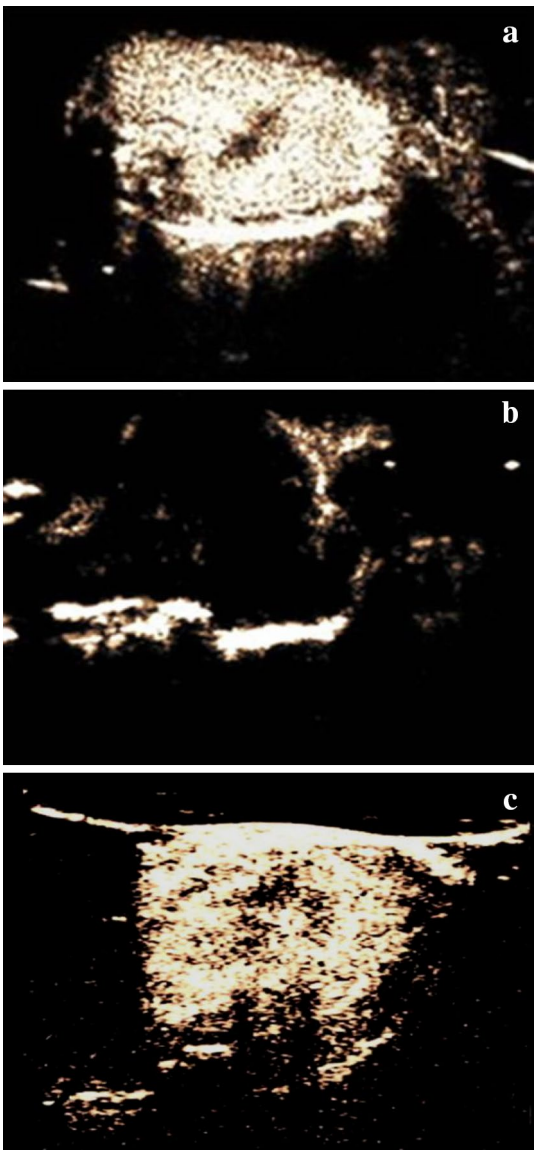

Fig. 3 Effects of UTMD on tumor microcirculation. Intense enhancement in control group (**a**), 30 min after UTMD, no enhancement in the whole tumor (**b**), 3 h after UTMD, the tumor circulation resumed (**c**). The representative images were captured at 22nd second in the CEUS procedure

Effect of UTMD on drug distribution

In the Endostar and EM groups, the drug content in the tumor tissue was measured at 0.37 ± 0.15 μg/gram protein and 0.42 ± 0.18 μg/gram protein, respectively. However, with intravenous injection of Endostar-conjugated MBs followed by ultrasound exposure, the drug content was significantly increased compared with both the Endostar and EM groups at 1.12 ± 0.43 μg/gram protein($P < 0.01$).

In vivo antitumor effects

In the control group, the MDA-MB-231 breast cancer cells continually grew following subcutaneous transplantation in the mice. The tumors showed apparent enhancement by CEUS. After five treatments the tumor blood perfusion was reduced, the CEUS parameters PI and AUC significantly decreased compared with the control group (Fig. 4; Table 2). Meanwhile, the tumor growth in the treatment groups were inhibited to varying degrees (Fig. 5).This was especially true in the EMUTMD group that had the highest TGIR and the tumor mass was significantly smaller($P < 0.01$) compared with both the Endostar and EM groups (Table 3).

Comparison of tumor MVD

The microvessels of the tumor were abundant in the control group with an MVD of $23.35 \pm 4.56/mm^2$. In the Endostar and EM groups, the tumor microvessel density was decreased and the MVD were calculated as $15.67 \pm 3.24/mm^2$ and $15.54 \pm 3.11/mm^2$, respectively. The MVD in the EMUTMD group was the lowest at $5.34 \pm 0.27/mm^2$, significantly lower ($P < 0.01$) compared with the control, Endostar, and EM groups (Figs. 6, 7).

Determination of VEGF gene expression

The VEGF gene expression was down-regulated in the Endostar treatment groups. For the EMUTMD group, the difference was statistically significant ($P < 0.05$) compared with

Table 1 Comparison of tumor CEUS parameters between Control and UTMD group (mean ± sd)

Group	TP (s)	MTT (s)	PI (10E-5 AU)	AUC (10E-5AU.s)	AUC-WI (10E-5AU.s)	AUC-WO (10E-5AU.s)
Control	20.5 ± 5.9	35.3 ± 6.7	10.8 ± 3.1	532.4 ± 62.5	119.5 ± 25.3	412.9 ± 46.7
UTMD 3 h	22.3 ± 6.4	38.2 ± 8.5	8.2 ± 2.6	389.2 ± 59.6	106.4 ± 22.5	282.8 ± 42.3

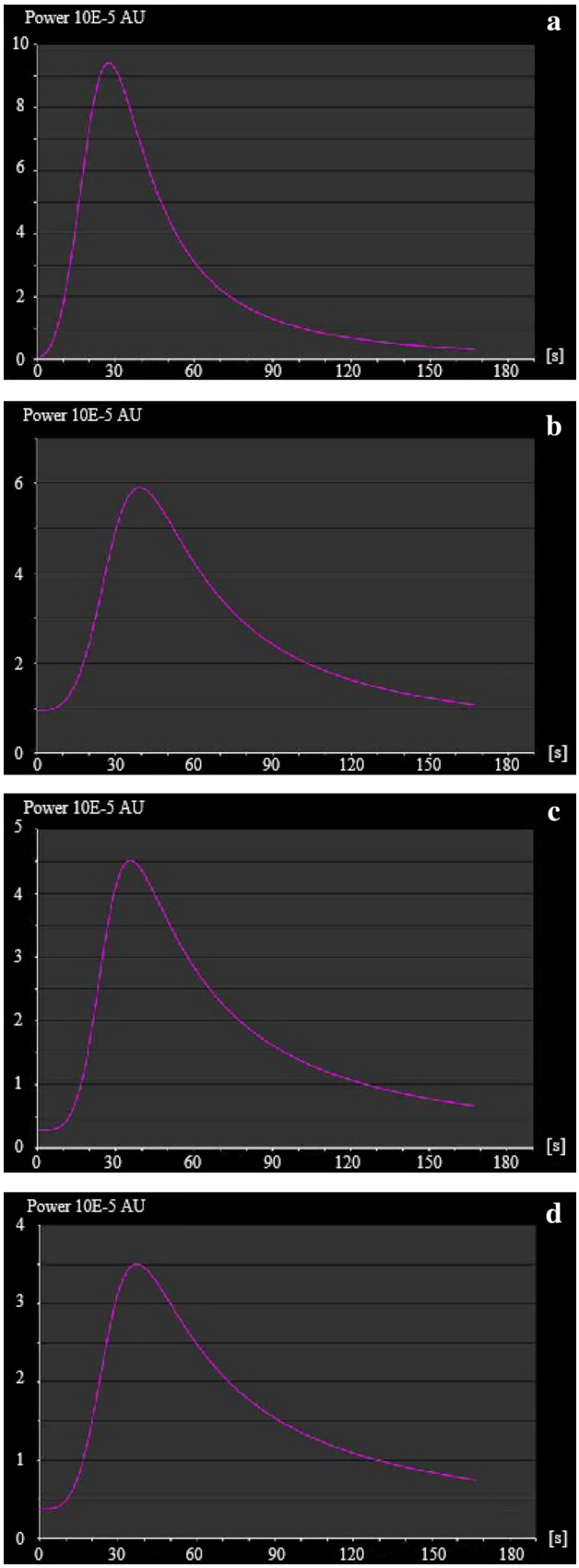

Fig. 4 The Time Intensity Curve of the tumor by CEUS. The AUC for control group (**a**), Endostar group (**b**), EM group (**c**) and EMUTMD group (**d**) were 412.2×10^{-5} AU.s, 310.6×10^{-5} AU.s, 309.1×10^{-5} AU.s and 219.8×10^{-5} AU.s, respectively

both the Endostar and EM groups and very statistically significant ($P<0.01$) compared with the control group (Fig. 8).

Discussion

Lipid or polymer shelled and inert gas filled MBs (2–4 μm in diameter) are excellent carriers for drugs and genes (Leon et al. 2018; Zhang et al. 2018; Yue et al. 2018; Tinkov et al. 2010). Many methods, for instance the biotin–avidin bridging method, covalent binding method, and electrostatic adherence have been developed for linking drugs to MBs (Avivi et al. 2005; Tan et al. 2003; Lindner et al. 2001). Among them, the biotin–avidin bridging chemistry method is considered an ideal approach for protein conjunction due to its high specificity and stability (Teulon et al. 2011). In addition, one avidin has four subunits and each one can combine with one biotin molecule, thus producing a cascade amplification effect and powerful combination capacity. In this study, Endostar was successfully linked to the lipid-shelled MBs with this binding method, and qualitatively confirmed by fluorescence microscopy and further quantitatively determined by ELISA.

Generally, the discontinuous capillaries in normal tissue have fenestrations of approximately 150 nm (Danquah et al. 2011), and the size of the gaps of cancer blood vessels has been estimated to be 100–600 nm (Maruyama 2011). Presently, the acoustic contrast agents used in the clinic are of micron grade, which cannot penetrate the vascular endothelial gap, nor be accurately targeted to cancer cells. We set the neovessel endothelial cells of breast cancer as the targeted treatment site, which allowed the prepared Endostar-conjugated MBs to efficiently perform their antiangiogenic effects.

Ultrasound exposure can produce thermal, cavitation, and mechanical effects in biological tissues. Combining MBs with ultrasound exposure improved the physical effects and the subsequent biological effects and is considered a promising technique for drug and gene delivery (Bastarrachea et al. 2017; Chen et al. 2017; Xiang et al. 2016). Among the physical effects, cavitation plays a key role. It causes vibration, expansion, and implosion of MBs along with multiple energy release behaviors such as high temperature, high voltage, and micro jetting. UTMD also induces biological effects, for example, microvessel wall rupture, tiny hematomas, and thrombi (Suzuki et al. 2010; Wand et al. 2010; Hwang et al. 2005). Although the destructive effect of UTMD is aggravated with the increase of injected MBs and the energy of ultrasonic irradiation (Miller et al. 2005),

Table 2 Comparison of the tumor CEUS parameters in different groups (mean ± sd)

Group	TP (s)	MTT (s)	PI (10E-5 AU)	AUC (10E-5AU.s)	AUC-WI (10E-5AU.s)	AUC-WO (10E-5AU.s)
Control	19.9 ± 4.7	33.0 ± 8.3	9.3 ± 2.6	412.0 ± 59.3	110.3 ± 20.5	301.7 ± 51.3
Endostar	20.5 ± 4.8	46.2 ± 9.9*	6.5 ± 1.9*#	330.9 ± 45.7*#	96.9 ± 29.4	234.0 ± 46.7*#
EM	20.7 ± 5.6	45.2 ± 9.6*	6.7 ± 2.1*#	319.8 ± 50.3*#	85.7 ± 25.7*#	234.1 ± 49.5*#
EMUTMD	23.1 ± 6.9	51.8 ± 8.7**	3.4 ± 0.9**	192.1 ± 29.6**	46.6 ± 19.3**	145.5 ± 30.2**

*$P < 0.05$, **$P < 0.01$, versus Control group, #$P < 0.05$ versus EMUTMD group

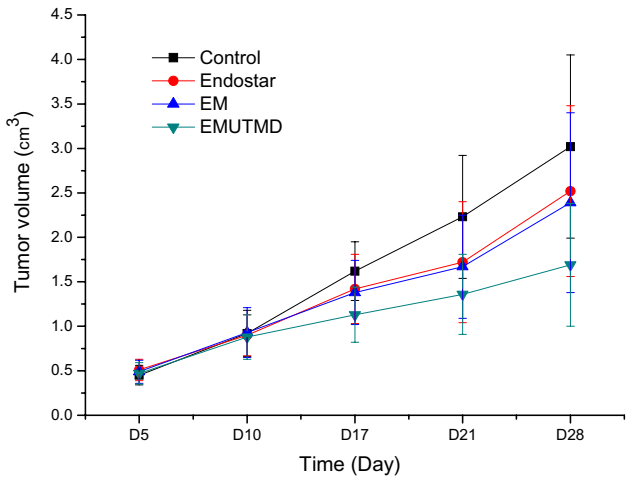

Fig. 5 The tumor volume with different treatment. The tumor volume increased persistently in the control group. In the Endostar and EM groups, the tumor growth was inhibited to some extent, while in EMUTMD group the mean tumor volume was minimal

Table 3 Antitumor effects on breast cancer xenografts (mean ± sd)

Group	Tumor mass (g)	TGIR (%)
Control	3.09 ± 1.12	–
Endostar	2.46 ± 1.05*#	20.39
EM	2.33 ± 1.18*#	24.60
EMUTMD	1.66 ± 0.84**	46.29

*$P < 0.05$, **$P < 0.01$, versus Control group, #$P < 0.05$ versus EMUTMD group

high ultrasonic dosage (including both ultrasound power and exposure time) may hurt the irradiated skin of nude mice and cause ulcers. After several trials, the ultrasound power was set as 0.75 W/cm^2 with sonication for 2 min (an irradiation of 10 s and an interval of 10 s for six cycles), and the results certified that it was safe and efficient for the animals. Chang, et al. also verified that UTMD with 1 MHz pulsed ultrasound 0.5 W/cm^2 for 30 s can enhance the gene transfection efficiency in ovarian cancer cells (Chang et al. 2013).

The ultrasound device mainly used in UTMD research was the clinic ultrasound diagnostic system (Kopechek et al. 2015; Bettinger et al. 2012). This equipment has an advantage that during the UTMD procedure the tissue perfusion can be monitored in real time. However, the acoustic beam produced from the ultrasound probe used in the clinic is very narrow: for example, the acoustic beam-width of an ultrasound probe (frequency 3.5–5.0 MHz) was less than 0.2 cm. Apparently, using this clinical ultrasonic diagnostic probe, UTMD can only act on tissue with a width of less than 0.2 cm at one time. The transplanted tumor size in this study for UTMD was over 1.0 cm, therefore, we used an ultrasound equipment that produced a cylindrical acoustic beam with an irradiation diameter about 3.0 cm, which can cover the whole tumor during UTMD.

CEUS is a newly developed ultrasound technique and has been used in clinical diagnosis and experimental research (Willmann et al. 2008; Deshpande et al. 2011). Using the MBs, CEUS can detect the blood flow at a speed of about 1 mm/s in microvessels (diameter about 10–30 μm) in real time. With the application of software, CEUS can quantitatively analyze a lot of parameters, including PI, TP, MTT, AUC, AUC-WI and AUC-WO. Therefore, CEUS has been widely applied to evaluate the microcirculation of tumors, liver, kidney, and other tissues (Lucidarme et al. 2006; Paprottka et al. 2010; Zhang et al. 2011). With CEUS we confirmed that UTMD can block the microcirculation in the entire tumor. However, the tumor microcirculation blocking was not persistent. With the prolonging of time, the tumor circulation gradually resumed.

Intravenously injected lipid-based microbubbles may be taken up by macrophages associated with the reticular endothelial system, for example, hepatic Kupffer cells and splenic macrophages (Sirsi etal. 2010), which would decrease the microbubbles distribution in the target tissue. The high conformational flexibility and hydrophilicity of PEG make the microbubbles stable and refrain from interactions with proteins in the blood (Salmaso et al. 2013). PEGylation creates a steric shield surrounding the microbubble, reducing opsonization and subsequent clearance by the reticular endothelial system (Butcher et al. 2016). In this study, the PEGylated phospholipid, DSPE-PEG2000 was used to prepare the Endostar-conjugated MBs to avoid the clearance by the reticular endothelial system, thus increasing the MBs distribution in the tumor tissue.

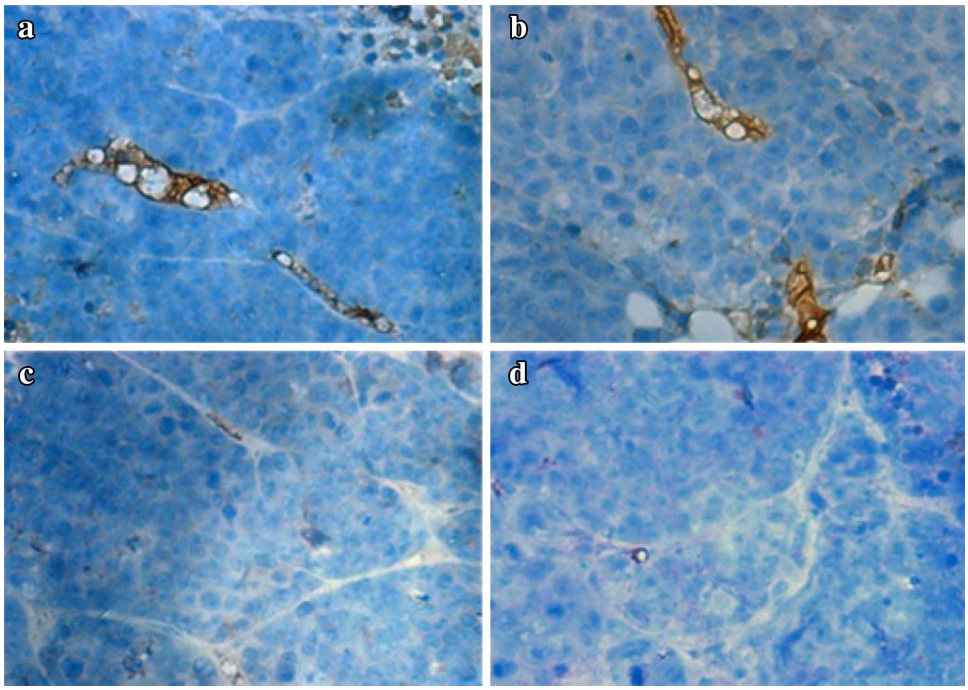

Fig. 6 Immunohistochemistry photo for MVD in different groups. Control group (**a**), Endostar group (**b**), Endostar-conjugated MBs (**c**), Endostar-conjugated MBs combining with UTMD (**d**)

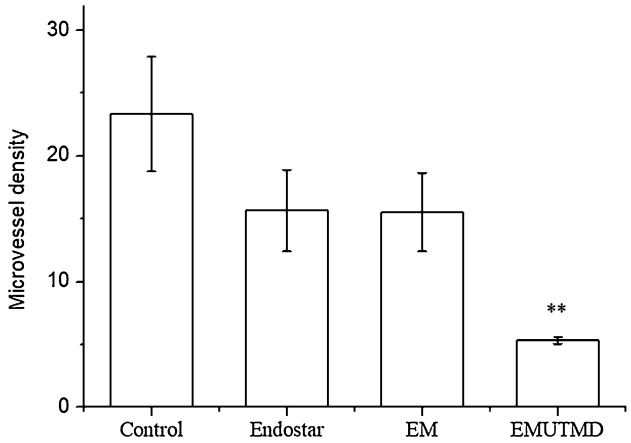

Fig. 7 MVD in MDA-MB-231 breast cancer tissue with different treatment. In EMUTMD group, the MVD was significantly lower than that in other groups (**$P<0.01$)

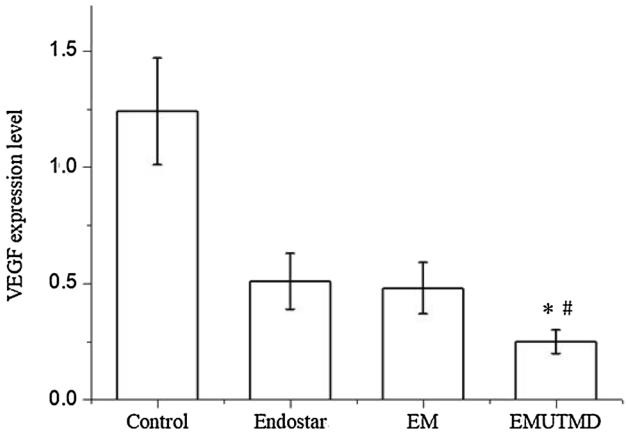

Fig. 8 Comparison of VEGF expression level in different groups. The VEGF expression level was significantly lower in the EMUTMD group than in the other groups (*$P<0.05$, $^{\#}P<0.01$)

UTMD can stimulate the permeabilization of the vessel wall and cell membranes (Fredenberg et al. 2011; Bekeredjian et al. 2007). With the rupture of the Endostar-conjugated MBs by UTMD, Endostar was released in the destroyed vessels, and the drug content detected by ELISA was about three times higher than in the Endostar group or EM group, further demonstrating that UTMD is an effective drug targeting delivery approach. Endostar-conjugated MBs combined with UTMD had effective antitumor function, and the TGIR was about two times higher than that in either the Endostar group or EM group. The MVD determination results confirmed that Endostar-conjugated MBs combined with UTMD inhibited tumor vessel generation. Two principal underlying mechanisms may explain the biological effects induced by UTMD and the symphysial antiangiogenesis by the targeted treatment of Endostar. During the process of tumor growth, the cells secrete numerous angiogenesis factors including VEGF, which stimulates the proliferation of vascular endothelial cells and enhances the generation of microvessels (Toi et al. 1994). With administration of Endostar-conjugated MBs, followed by UTMD, the tumor VEGF expression level was significantly down-regulated, which may be a potential mechanism for antiangiogenesis.

In conclusion, UTMD can block the tumor microcirculation, increase drug release in the targeted tumor, and improve the antiangiogenic and antitumor effects of Endostar. This may be a potentially efficacious treatment strategy for drug-resistant and other refractory breast cancers.

Acknowledgements This work was supported by the Key Project for Youth Academic Talents (2015-ZQN-ZD-13), Medical Innovation Project (2015-CXB-17) from Health and Family Planning Commission of Fujian Province and the General Program (2016J01710) of Science and Technology Department of Fujian Province of China.

Compliance with ethical standards

Conflict of interest The authors declare that they have no competing interest.

References

Avivi LS, Gedanken A (2005) The preparation of avidin microspheres using the sonochemical method and the interaction of the microspheres with biotin. Ultrason Sonochem 12(5):405–409

Bastarrachea RA, Chen J, Kent JW Jr et al (2017) Engineering brown fat into skeletal muscle using ultrasound-targeted microbubble destruction gene delivery in obese Zucker rats: Proof of concept design. Iubmb Life 69(9):745–755

Bauer KR, Brown M, Cress RD et al. (2007) Descriptive analysis of estrogen receptor (ER)-negative, progesterone receptor (PR)-negative, and HER2-negative invasive breast cancer, the so-called triple-negative phenotype: a population-based study from the California. Cancer Regist Cancer 109(1):1721–1728

Bekeredjian R, Kroll RD, Fein E et al (2007) Ultrasound targeted microbubble destruction increases capillary permeability in hepatomas. Ultrasound Med Biol 33(10):1592–1598

Bettinger T, Bussat P, Tardy I et al (2012) Ultrasound molecular imaging contrast agent binding to both E- and P-selectin in different species. Invest Radiol 47(9):516–523

Butcher NJ, Mortimer GM, Minchin RF (2016) Drug delivery: unravelling the stealth effect. Nat Nanotechnol 11:310–311

Carmeliet P, Jain RK (2011) Principles and mechanisms of vessel normalization for cancer and other angiogenic diseases. Nat Rev Drug Discov 10(6):417–427

Chang S, Guo J, Sun J et al (2013) Targeted microbubbles for ultrasound mediated gene transfection and apoptosis induction in ovarian cancer cells. Ultrason Sonochem 20(1):171–179

Chen S, Grayburn PA (2017) Ultrasound-targeted microbubble destruction for cardiac gene delivery. Methods Mol Biol 1521:205–218

Danquah MK, Zhang XA, Mahato RI (2011) Extravasation of polymeric Nanomedicines across tumor vasculature. Adv Drug Deliv Rev 63(8):623–639

De Temmerman ML, Dewitte H, Vandenbroucke RE et al (2011) mRNA-Lipoplex loaded microbubble contrast agents for ultrasound-assisted transfection of dendritic cells. Biomaterials 32(34):9128–9135

Delalande A, Kotopoulis S, Postema M et al (2013) Sonoporation: mechanistic insights and ongoing challenges for gene transfer. Gene 525(2):191–199

Dent R, Trudeau M, Pritchard KI et al (2007) Triple-negative breast cancer: clinical features and patterns of recurrence. Clin Cancer Res 13:4429–4434

Deshpande N, Ren Y, Foygel K et al (2011) Tumor angiogenic marker expression levels during tumor growth: longitudinal assessment with molecularly targeted microbubbles and US imaging. Radiology 258(3):804–811

Fredenberg S, Wahlgren M, Reslow M et al (2011) The mechanisms of drug release in poly(lactic-co-glycolic acid)-based drug delivery systems—a review. Int J Pharm 415(1–2):34–52

Fukumura D, Jain RK (2007) Tumor microvasculature and microenvironment: targets for anti-angiogenesis and normalization. Microvasc Res 74(2–3):72–84

Hwang JH, Brayman AA, Reidy MA et al (2005) Vascular effects induced by combined 1-MHz ultrasound and microbubble contrast agent treatments in vivo. Ultrasound Med Biol 31(4):553–564

Karaca O, Ertekin T, Canoz O et al (2012) Effect of endostatin on 1,2-dimethylhydrazine-induced colon tumor in mice. Toxicol Ind Health 28(1):21–26

Keam B, Im SA, Lee KH et al (2011) Ki-67 can be used for further classification of triple negative breast cancer into two subtypes with different response and prognosis. Breast Cancer Res 13(2):R22

Kopechek JA, Carson AR, McTiernan CF et al (2015) Ultrasound targeted microbubble destruction-mediated delivery of a transcription factor decoy inhibits STAT3 signaling and tumor growth. Theranostics 5(12):1378–1387

Leon AD, Perera R, Nittayacharn P et al (2018) Ultrasound contrast agents and delivery systems in cancer detection and therapy. Adv Cancer Res 139:57–84

Lindner JR, Song J, Christiansen J et al (2001) Ultrasound assessment of inflammation and renal tissue injury with microbubbles targeted to P-selectin. Circulation 104(17):2107–2112

Lucidarme O, Kono Y, Corbeil J et al (2006) Angiogenesis: noninvasive quantitative assessment with contrast-enhanced functional US in murine model. Radiology 239(3):730–739

Luo H, Xu M, Zhu X et al (2015) Lung cancer cellular apoptosis induced by recombinant human endostatin gold nanoshell-mediated near-infrared thermal therapy. Int J Clin Exp Med 8(6):8758–8766

Maruyama K (2011) Intracellular targeting delivery of liposomal drugs to solid tumors based on EPR effects. Adv Drug Deliv Rev 63(3):161–169

Matsumoto G, Hirohata R, Hayashi K et al (2014) Control of angiogenesis by VEGF and endostatin-encapsulated protein microcrystals and inhibition of tumor angiogenesis. Biomaterials 35(4):1326–1333

Miller DL, Li P, Dou C et al (2005) Influence of contrast agent dose and ultrasound exposure on cardiomyocyte injury induced by myocardial contrast echocardiography in rats. Radiology 237(1):137–143

Molinari F, Meiburger KM, Giustetto P et al (2014) Quantitative assessment of cancer vascular architecture by skeletonization of high-resolution 3-D contrast-enhanced ultrasound images: role of liposomes and microbubbles. Technol Cancer Res Treat 13(6):541–550

O'Reilly MS, Boehm T, Shing Y et al (1997) Endostatin: an endogenous inhibitor of angiogenesis and tumor growth. Cell 88(2):277–285

Paprottka PM, Cyran CC, Zengel P et al (2010) Non-invasive contrast enhanced ultrasound for quantitative assessment of tumor microcirculation. Contrast mixed mode examination vs. only contrast enhanced ultrasound examination. Clin Hemorheol Microcirc 46(2–3):149

Salmaso S, Caliceti P (2013) Stealth properties to improve therapeutic efficacy of drug nanocarriers. J Drug Deliv 2013:374252

Sharma G, Mirza S, Parshad R,et al (2011) Clinical significance of maspin promoter methylation and loss of its protein expression in invasive ductal breast carcinoma: correlation with VEGF-A and MTA1 expression. Tumour Biol 32(1):23–32

Sirsi S, Feshitan J, Kwan J et al (2010) Effect of microbubble size on fundamental mode high frequency ultrasound imaging in mice. Ultrasound Med Biol 36(6):935–948

Suzuki J, Ogawa M, Takayama K et al (2010) Ultrasound microbubble mediated intercellular adhesion molecule small interfering ribonucleic acid transfection attenuates neointimal formation after arterial injury in mice. J Am Coil Cardiol 55(9):904–913

Tan PH, Manunta M, Ardjomand N et al (2003) Antibody targeted gene transfer to endothelium. J Gene Med 5(4):311–323

Teulon JM, Delcuze Y, Odorico M et al (2011) Single and multiple bonds in (strept) avidin–biotin interactions. J Mol Recognit 24(3):490–502

Tinkov S, Coester C, Serba S et al (2010) New doxorubicin-loaded phospholipid MBs for targeted tumor therapy: in-vivo characterization. J Control Release 148(3):368–372

Toi M, Hoshina S, Takayanagi T et al (1994) Association of vascular endothelial growth factor expression with tumor angiogenesis and with early relapse in primary breast cancer. Jpn J Cancer Res 85(10):1045–1049

Wand Y, Zhou J, Zhang Y et al (2010) Delivery of TFPI-2 using SonoVue and adenovirus results in the suppression of thrombosis and aerial restenosis. Exp Biol Med (Maywood) 235(9):1072–1081

Wen Q, Wan S, Liu Z et al (2014) Ultrasound contrast agents and ultrasound molecular imaging. J Nanosci Nanotechnol 14(1):190–209

Willmann JK, Paulmurugan R, Chen K et al (2008) US imaging of tumor angiogenesis with microbubbles targeted to vascular endothelial growth factor receptor type 2 in mice. Radiology 246(2):508–518

Wu XL Kim JH, Koo H et al (2010) Tumor-targeting peptide conjugated pH-responsive micelles as a potential drug carrier for cancer therapy. Bioconjug Chem 21(2):208–213

Xiang X, Tang Y, Leng Q et al (2016) Targeted gene delivery to the synovial pannus in antigen-induced arthritis by ultrasound-targeted microbubble destruction in vivo. Ultrasonics 65:304–314

Xu M, Xu CX, Bi WZ et al (2013) Effects of endostar combined multidrug chemotherapy in osteosarcoma. Bone 57(1):111–115

Yuan J, Wu CW, Liu ZJ et al (2010) Observation of the antitumor effect of endostar combined with docetaxel under different administration sequences. Zhonghua Zhong Liu Za Zhi 32(8):580–585

Yue P, Gao L, Wang X et al (2018) Ultrasound-triggered effects of the microbubbles coupled to GDNF- and Nurr1-loaded PEGylated liposomes in a rat model of Parkinson's disease. J Cell Biochem 119(6):4581–4591

Zhai J, Yang X, Zhang Y et al (2013) Reduced expression levels of the death-associated protein kinase and E-cadherin are correlated with the development of esophageal squamous cell carcinoma. Exp Ther Med 5(3):972–976

Zhang MB, Qu EZ, Liu JB et al (2011) Quantitative assessment of hepatic fibrosis by contrast-enhanced ultrasonography. Chin Med Sci J 26(4):208–215

Zhang J, Wang S, Deng Z et al (2018) Ultrasound-triggered drug delivery for breast tumor therapy through iRGD-targeted paclitaxel-loaded liposome- microbubble complexes. J Biomed Nanotechnol 14(8):1384–1395